Journal of Alloys and Compounds 700 (2017) 130–137

Contents lists available at ScienceDirect

Journal of Alloys and Compounds

journal homepage: http://www.elsevier.com/locate/jalcom

Photoluminescence properties of (Eu, Tb, Tm) co-doped $PbMoO_4$ obtained by sonochemical synthesis

G.M. Gurgel [a], L.X. Lovisa [a, *], L.M. Pereira [a], F.V. Motta [a], M.S. Li [b], E. Longo [c], C.A. Paskocimas [a], M.R.D. Bomio [a, **]

[a] DEMAT, CT, UFRN, Av. Sen. Salgado Filho, 3000, CEP 59072-970 Natal, RN, Brazil
[b] IFSC, USP, Av. Trabalhador São Carlense, 400, CEP 13566-590 São Carlos, SP, Brazil
[c] LIEC, IQ, UNESP, Rua Francisco Degni s/n, CEP 14801-907 Araraquara, SP, Brazil

ARTICLE INFO

Article history:
Received 13 September 2016
Received in revised form
23 December 2016
Accepted 30 December 2016
Available online 6 January 2017

Keywords:
$PbMoO_4$
Earth rare
Sonochemistry
Photoluminescence

ABSTRACT

The $PbMoO_4$ co-doped with Tm^{3+}, Tb^{3+} Eu^{3+} with scheelita structure was synthesized by the sonochemical method. The photoluminescent properties, structural and color coordinates emitted by phosphors were investigated. The structural analysis of the crystal and the changes in lattice parameters confirm that the rare earth ions (RE^{3+}) were successfully introduced into the host of the $PbMoO_4$. The relationship between energy gap (Egap) and the concentration of RE^{3+} ions was also discussed, the Egap is significantly influenced by the degree of structural order-disorder present in the crystal lattice. The $PbMoO_4$:RE^{3+} shows light emission in green. Under UV excitation, Photoluminescence (PL) shows a broad band centered at 520 nm and smaller bands belonging to transitions of RE^{3+}: $^1G_4 \rightarrow {}^3F_4$ and $^1D_2 \rightarrow {}^3H_4$ at 480 and 533 nm (Tm^{3+}), $^5D_4 \rightarrow {}^7F_j$ (j = 6, 5) at 493 and 550 nm (Tb^{3+}) $^5D_0 \rightarrow 7Fj$ (j = 1, 2, 4) 593, 615 and 702 nm (Eu^{3+}).

1. Introduction

The relationship between morphology and particle properties has attracted considerable attention from many researchers lately [1–3] because of the potential of these materials to be applied in multiple areas. Groups of functional materials are emerging based on the control of particle size and morphology. These characteristics are controlled from the synthesis parameters of the materials, such as: reagent concentration, precursor pH, reaction temperature and time and synthesis method [4].

Molybdates are ternary compounds of the general formula $AMoO_4$ (A = Ca, Sr, Ba, Pb, Cd, etc.) with a tetragonal structure of the scheelite type. The lead molybdate ($PbMoO_4$) is studied as potential material in photoluminescence, catalysis and scintillating materials [5–7]. The $PbMoO_4$ presents a $I4_1/a$ a space group and a C_{4h}^6 symmetry group with two formula units per primitive cell [8,9] and a specific feature of these systems is the existence of two different clusters in a crystal lattice, in which each Mo is surrounded by four equivalent O atoms composing the $[MoO_4]^{2-}$ tetrahedral configuration and each divalent metal, Pb, shares corners with eight adjacent O atoms, forming a $[PbO_8]^{2-}$ configuration.

Several methods were used to obtain lead molybdates such as microwave irradiation, sonochemical, co-precipitation and solvothermal [6,10–12]. The sonochemical method is a potential chemical route for the production of inorganic materials in the nano/micrometer scale [13–15]. The action of ultrasonic irradiation in the process of material synthesis results from a phenomenon known as acoustic cavitation. In this case, the formation, growth and implosive collapse of the bubbles in the solution occurs. The collapse of these bubbles allows the release of high energy in the form of high temperatures at localized points favoring that the formation reaction of the materials occurs. The extreme conditions of temperature (>5000 K), pressure (>20 MPa) and cooling rate (10^1 K.s^{-1}) that the reaction medium can attain during acoustic cavitation may lead to the achievement of many superior properties by the irradiated solution [16]. Among the advantages that the sonochemical method presents are the rapid reaction rate, the control of the synthesis parameters, formation of uniform particles, with strict size distribution and high purity [17].

Inorganic materials doped with rare earth ions (RE^{3+}) have been extensively studied based on their f - f type transitions due to their

* Corresponding author.
** Corresponding author.
E-mail address: lauraengmat@hotmail.com (L.X. Lovisa).

http://dx.doi.org/10.1016/j.jallcom.2016.12.409
0925-8388/

wide application in the field of illumination [18,19]. The electronic transitions and structural defects that RE^{3+} dopants cause within a lattice are responsible for generating characteristics at the energy levels of the crystal that helps design phosphors for visualization applications. Thulium (Tm^{3+}), terbium (Tb^{3+}) and europium (Eu^{3+}) are ions already used in the doping process and have characteristic emissions in blue, green and red, respectively [20–22].

In this study, $PbMoO_4$ particles and $PbMoO_4$ co-doped with RE^{3+} (Tm^{3+}, Tb^{3+} and Eu^{3+}) were successfully synthesized by the sonochemical method. Characterizations: structural, morphological and spectroscopy of the samples were performed by XRD, absorption Uv–vis spectroscopy, FEG-SEM and Photoluminescence. The effect of the concentration of the dopants discussed. The $PbMoO_4$: RE is shown as a promising candidate for functional applications.

2. Material and methods

2.1. Materials

The materials used in the syntheses were: molybdic acid (Alfa Aesar, 85%), lead nitrate (Aldrich, 99%), rare earth oxides: Tm_2O_3 (Aldrich 99.9%), Tb_4O_7 (Aldrich 99.9%) and (Eu_2O_3 - Aldrich 99.9%) and ammonium hydroxide (Synth, 30% NH_3). All reagents used in the experiment were of analytical grade.

2.2. Methods

The $PbMoO_4$: RE particles were prepared by the sonochemical method [23]. Initially, it was prepared a molybdic acid solution (5×10^{-3} mol) in 50 ml of deionized water. Then, the lead nitrate (5×10^{-3} mol) was added to the solution. After the complete dissolution of the cations (Mo, Pb), the rare earth ions ($RE^{3+} = Eu^{3+}$, Tm^{3+}, Tb^{3+}) were added to the reaction. The pH of the solution was adjusted to 9 by the addition of ammonium hydroxide, observing the precipitate formation. A europium solution, thulium solution and terbium solution were prepared through the dissolution of the respective oxides in nitric acid. The resulting solution was exposed to high intensity ultrasound irradiation (Branson Digital Sonifier) with 70% amplitude in a continuous mode. After that, the products were separated from the solution by centrifugation, washed with deionized water for four times to remove any residual material, and then dried at 80 °C for 12 h. The time of synthesis was 30 and 45 min for each processed composition. The concentration of Tb^{3+} and Tm^{3+} was maintained to 1 mol% for these dopant in all compositions, the Eu^{3+} concentration varied among 0.5, 1 and 1.5 mol% in order to assess its effect on the photoluminescence behavior.

2.3. Characterization of particles $PbMoO_4$: RE

The phases present in the ceramic powder were investigated by X-ray diffraction (XRD) using a Shimadzu diffractometer, XRD-7000 model with radiation CuKα (λ = 1.5406 Å) in the range 2θ from 10° to 90° and the step speed of 1°/min. The reflectance spectra in the Uv–visible particles were performed using a Cary equipment, 5G model. The distribution of particle size and morphology were investigated by Supra 35 VP-FEG-SEM (Carl Zeiss, Germany) operating at 6 kV. The photoluminescence spectra were obtained by the monochromator ThermalJarrel AshMonospec 27 and the Hamatsu R446 photomultiplier.

The excitation source used in the samples was a wavelength of 350.7 nm of a laser with krypton ions (CoherentInnova) with a power of about 13.3 mW, all measurements were performed at room temperature. UV–vis and PL spectra were taken three times for each sample to ensure the reliability of the measurements. To characterize the color of light emmited by the samples, it was calculated the chromaticity coordinates, using the PL emission spectrum shown in Fig. 4. The chromaticity coordinates in red (X), green (Y), and blue (Z) were determined according to the International Commission on Illumination system in 1968 [24,25] using the following relationship:

$$x = \frac{X}{(X+Y+Z)}\ y = \frac{Y}{(X+Y+Z)}\ z = \frac{Z}{(X+Y+Z)} \quad (1)$$

where the parameters X, Y and Z are the following spectral integrals

$$X = \int xP(\lambda)d\lambda\ Y = \int yP(\lambda)d\lambda\ Z = \int zP(\lambda)d\lambda \quad (2)$$

X, Y and Z are spectral functions. The integrals (2) were calculated in the spectral range 350 and 800 nm. P (λ) is the luminescence spectrum of the samples, which shows the intensity emitted. The function P (λ) is empirically determined, the values of λ for he components x, y and z are 599, 555 and 446 nm, respectively [26] and X, Y and Z are functions for different spectral. As (2) they were calculated in the spectral range of 350 and 800 nm.

3. Results and discussion

3.1. X-ray diffraction

The patterns of X-ray diffraction of the samples synthesized by the sonochemical method are shown in Fig. 1. All diffractions detected were indexed as a tetragonal crystal structure of scheelite type which is according to the crystallographic JCPDS card (44-1486), indicating that the RE^{3+} dopant did not induce significant changes in the matrix structure. The XRD patterns for the $PbMoO_4$: RE represented in Fig. 1 are for different concentrations of Eu^{3+}.The synthesis time was another parameter analyzed. Fig. 1a and (b) correspond to the syntheses performed at 30 and 45 min respectively. The relative intensities and the narrow diffraction peaks indicate a high crystallinity of the particles, suggesting an ordered structure over long distances.

The average crystallite size (D) estimated by the Scherrer equation and the changes of lattice parameters and unit cell volume depending on the concentration of RE^{3+} ions are shown in Table 1.

Since the ionic radius of RE^{3+} (Tm^{3+} = 0.0869 nm, Tb^{3+} = 0.0923 nm and Eu^{3+} = 0.0947 nm) are smaller than the ionic radius of Pb^{2+} (0.119 nm) parameters lattice (a, c) and unit cell volume (V) decreases with increasing concentration of RE^{3+} [27]. This behavior shows that RE^{3+} ions can easily enter the host lattice of the $PbMoO_4$. The lattice parameters obtained from the XRD of the $PbMoO_4$ crystals are very close to the results reported in the literature [11]. However, small variations in the values may be attributed to the type synthesis adopted and the processing conditions of the material.

The Egap of the particles of $PbMoO_4$ was estimated from results obtained by diffuse reflectance spectroscopy by plotting the Kubelka-Munk vs Egap function (eV) extrapolating the linear part of the curve $F(R)^2 = 0$, as shown in Fig. 2. The ratio of Kubelka-Munk [28] is described in equation (3):

$$F(R) = \frac{k}{s} = \frac{(1-R)^2}{2R} \quad (3)$$

Where F(R) is the Kubelka-Munk function, R is the percentage of reflected light, k is the molar absorption coefficient and s is spreading coefficient. A incident photon energy (hn) and the energy bandgap (Egap) are related to the Kubelka-Munk function as follows: $[F(R)\ hv]^p = A$ (hv - Egap), where A is a constant which

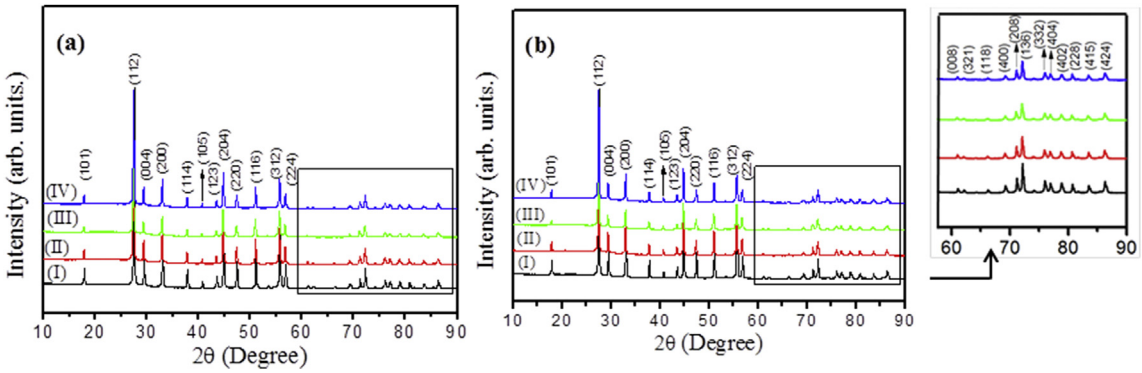

Fig. 1. X-ray diffractogram of the $PbMoO_4$ materials for different concentrations of Eu^{3+} [(I) 0, (II) 0.5, (III) 1 and (IV) 1.5 mol %], synthesis time: (a) 30 min and (b) 45 min.

Table 1
Particle crystallographic data of $PbMoO_4$:RE.

Conditions	D (nm)	a = b (Å)	c (Å)	V (Å)^3
PMO pure – 30min	52.00	5.433	12.14	358.50
PMO: 1% Tm 1% Tb 0.5%Eu – 30min	52.93	5.431	12.13	357.78
PMO: 1% Tm 1% Tb 1%Eu – 30min	59.40	5.427	12.14	357.80
PMO: 1% Tm 1% Tb 1.5%Eu – 30min	46.77	5.428	12.11	356.80
PMO pure – 45min	58.43	5.432	12.16	358.86
PMO: 1% Tm 1% Tb 0.5%Eu - 45min	46.65	5.419	12.11	355.87
PMO: 1% Tm 1% Tb 1%Eu – 45min	41.37	5.417	12.12	355.84
PMO: 1% Tm 1% Tb 1.5%Eu – 45min	59.41	5.410	12.14	355.31
[Ref.] JCPDS no. 44-1486	–	5.433	12.11	357.46

depends on the transition probabilities and p is the power ratio that is related to the process of optical absorption, p is equal to 1/2 or 2 for direct or indirect allowed transitions, respectively. According to Lacomba-Perales et al., the molybdates with tetragonal structure scheelite type present a direct allowed electronic transition (p = 1/2) [29]. The estimated values of Egap for $PbMoO_4$ particles pure and co-doped with RE are shown in Fig. 2. It is observed that the values obtained are in accordance to the ones found in Ref. [5]. The gap energy depends on the degree of structural order-disorder present in the crystal lattice. The increase of RE^{3+} ions in the $PbMoO_4$ structure causes a reduction in its structural organization due to the appearance of intermediate levels in the forbidden band [30]. Therefore, a considerable reduction in the optical band-gap is probably linked to exchange ordered complex clusters to disordered complex clusters. In this typical semiconductor, the $PbMoO_4$ crystal lattice can have different types of electronic structure characteristics such as intercluster (intermediary range) and intracluster (local range) interactions, which can be due to three different sources: orientation, induction, and dispersion interactions [31].

From the absorption edges of the sample band gap $PbMoO_4$ obtained was estimated at between 3.18 and 3.24 eV, which is in good agreement with the values obtained previously reported data band gap [32]. The Egap values showed small differences which may be related to other experimental aspects including material preparation, particle morphology and synthesis processing time.

Fig. 3 shows the photoluminescence spectrum of pure $PbMoO_4$. The PL emission for particles was obtained using a laser with a wavelength equal to 350.7 nm, at environment temperature. It is noted that $PbMoO_4$ has an emission band with a predominantly green emission region, as shown in previous studies [33].

The PL spectrum shows a broad band between 400 and 750 nm. The curve in Fig. 3 shows a peak emission at 520 nm, which can be attributed to the charge transfer transitions within the $[MoO_4]$ clusters. This behavior can be related to the existence of structural defects of the Frenkel type (oxygen ions are out of their net position generating oxygen vacancies simultaneously) [34]. These results indicate that the photoluminescence properties of $PbMoO_4$ are very sensitive to the structure and heavily dependent on structural defects. The result of the deconvolution performed in $PbMoO_4$ emission spectrum through the Peak Fit Program. Version 4.12 shows that broadband was broken down into four components in the range of blue, green, orange and red.

Some theories have been proposed to explain the PL emission behavior of molybdates. Blasse and Grabmaier [35] claim that the PL emission arises from a return of radiative emission is in competition with the non-radiative decay to the ground state. This non-radiative process leads to vibration and heating of the crystalline material lattice. From theoretical studies of the photoluminescence of $CaMoO_4$, Campos et al. [36] argue the existence of MoO_3 and MoO_4 distorted in lattice clusters cause the emergence of intermediate levels within the band gap, the 2p oxygen states are located near the valence band and the states 4d Mo are located below conduction band. This polarization induces a discontinuity in symmetry and the presence of localized energy levels contributes to the trapping of electrons (e^-) by the holes (h^+). According Spassy et al. [37] attribute the maximum emission at 490 nm to radiative transitions in complexes of $[MoO_4]^{2-}$, and assigns of the cation (Pb^{2+}) in $PbMoO_4$ crystals participate as emission centers, responsible for photoluminescence.

The PL results for co-doped samples at different concentrations are shown in Fig. 4. The peaks detected at 480 and 533 nm correspond to transitions of Tm^{3+} $^1G_4 \rightarrow {}^3F_4$ and $^1D_2 \rightarrow {}^3H_5$ [38] respectively. The peaks found at 493 and 550 nm are associated with transitions of Tb^{3+} $^5D_4 \rightarrow {}^7F_j$ (j = 6, 5) [39] respectively. The peaks observed at 593, 615 and 702 nm are related to transitions of Eu^{3+} $^5D_0 \rightarrow {}^7F_j$ (j = 1, 2, 4) [40] respectively. It is observed that the transitions of the type f → f of the RE^{3+} present in the emission spectrum are provided in the form of very discrete peaks at specific positions which are characteristic of these elements. It appears that this behavior was strongly influenced by photoluminescent performance displayed by the matrix.

The PL intensity observed by $PbMoO_4$ was so expressive that resulted in an overlap of the peaks f → f of RE^{3+}.There are several cases reported in the literature trying to explain the reasons for the photoluminescent properties in the $PbMoO_4$. Wu et al. [41] ensures that electronic transitions type $^1T_2 \rightarrow {}^1A_1$ within the tetrahedral groups $[MoO_4]^{2-}$ are responsible for the photoluminescence emission in the range of blue. Loo [42–44] assigns the photoluminescent emission in blue to isolated transitions of groups $[MoO_4]^{2-}$ and the emission in green to the overlapping of two bands, which is originated by transferring an electron occupying an orbital essentially character with Pb^{2+} to an adjacent vacant orbital

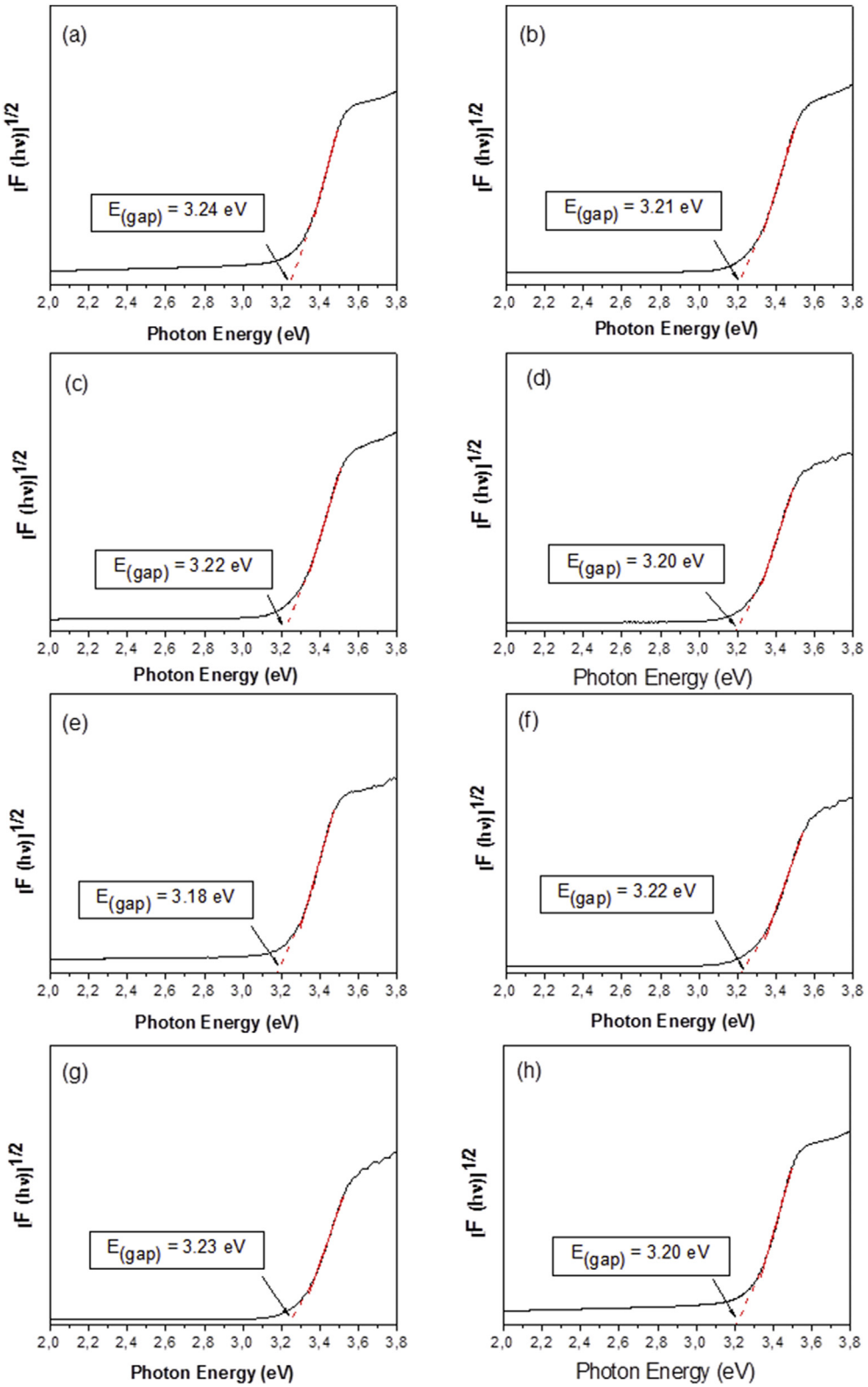

Fig. 2. Determination of the gap by Wood and Tauc method for particles synthesized at different times: (a) pure 30 min, (b) pure 45 min (c) 0.5% Eu 30 min (d) 0.5% Eu 45 min, (e) 1% Eu 30 min (f) 1% Eu 45 min, (g) 1.5% Eu 30 min and (h) 1.5% Eu 45 min.

of a $[MoO_4]^{2-}$ group, with a character predominantly of d-orbitals. Ryu et al. [45] and Yang et al. [46] relates the emergence of photoluminescent properties of molybdates with their morphology, crystallinity degree, and particle size.

The color coordinate is one of the important factors to evaluate the phosphors performance. Fig. 5 shows the chromaticity coordinates (x, y) of pure and co-doped samples $PbMoO_4$ produced in 30 and 45 min. It is observed that all samples showed emission in

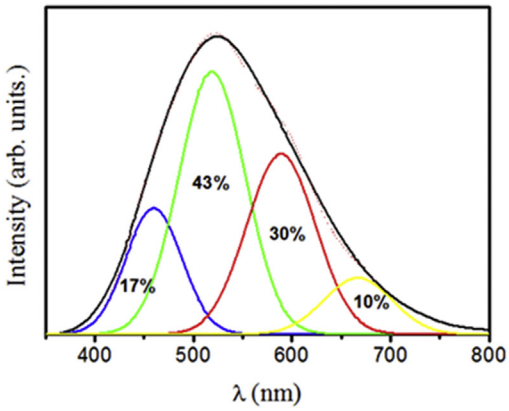

Area	Color	Center (nm)
17%	Blue	458
43%	Green	520
30%	Orange	590
10%	Red	667

Fig. 3. $PbMoO_4$ emission spectrum pure synthesized 45 min; deconvolution of the band with their contribution percentages in the visible range.

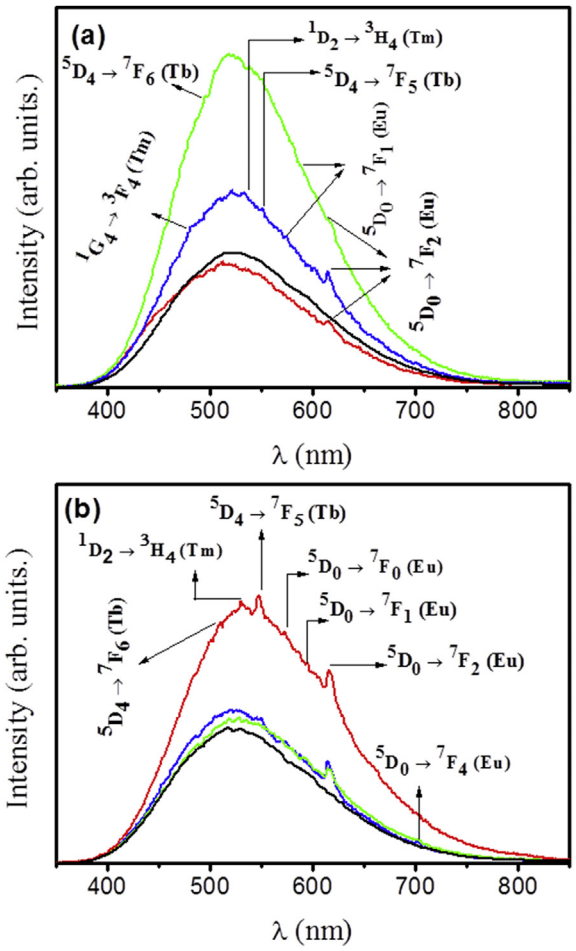

Fig. 4. $PbMoO_4$ emission spectrum pure and co-doped; (a) 30 min and (b) 45 min.

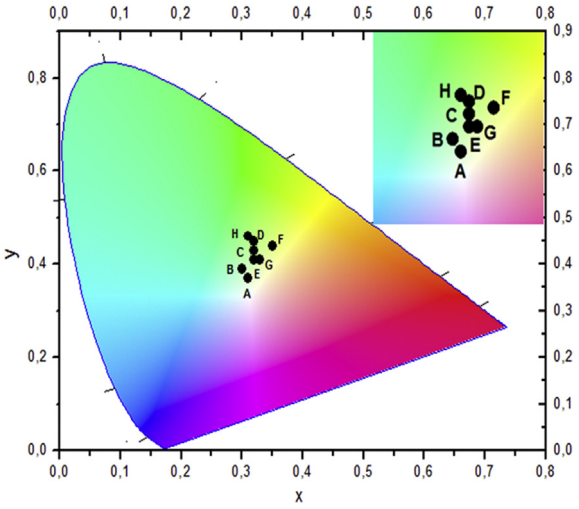

Fig. 5. Graph of CIE pure and co-doped $PbMoO_4$ in 30 and 45 min.

Table 2
CIE coordinates for pure and co-doped in 30 and 45 min.

Code	Samples	Coordinates (x,y)		Color
A	PMO pure 30 min	0,31	0,37	Green
B	PMO: 1% Tm 1% Tb 0.5%Eu – 30min	0.30	0.39	
C	PMO: 1% Tm 1% Tb 1%Eu – 30min	0.32	0.43	
D	PMO: 1% Tm 1% Tb 1.5%Eu – 30min	0.32	0.45	
E	PMO pure 45min	0.32	0.42	
F	PMO: 1% Tm 1% Tb 0.5%Eu – 45min	0.35	0.44	
G	PMO: 1% Tm 1% Tb 1%Eu – 45min	0.33	0.42	
H	PMO: 1% Tm 1% Tb 1.5%Eu – 45min	0.31	0.46	

the green region due to a higher contribution of around 520 nm as previously shown in Fig. 3. Table 2 lists the x, y values and color emitted for each sample.

The introduction of a dopant rare earth type in the host causes distortions in the lattice in the host material. This is because the ion characteristics substituent (RE^{3+}) is different from the replaced ion (Pb^{2+}). Some important factors that should be observed for the solubility of (RE^{3+}) in the matrix, they are: proximity of the size of the ionic radius of RE^{3+} and Pb^{2+}, the valence proximity and has the same crystal structure. The vacancy generation in the material is a mechanism to neutralize the electrical charges due to the replacement $Pb^{2+} \rightarrow RE^{3+}$. These types of structural defects are responsible for the facilitation of electronic transitions within the band gap. There is the XRD results that there is no intermediate stage of formation of rare earth elements. May so say that all the dopants have been successfully introduced into the $PbMoO_4$. The presence of rare earths is perceived through its specific transitions in emission spectra, shown in Fig. 4. An important contribution of the host is low phonon energy, which is related to non-radiative transitions, minimizing relaxation rates multiphonon thereby increasing the quantum efficiency.

Fig. 6 shows the FEG-SEM micrographs of particles of $PbMoO_4$: RE synthesized at different process times and with different amounts (mol %) of doping. Microscopic characterization of the $PbMoO_4$:RE particles is important for understanding of morphological evolution process of the particles according to the parameters investigated: synthesis time and concentration of RE.

It is observed in the image forming microparticle agglomerates. Of these microparticles coalesce in an oriented mode, these crystals grow in a definite direction as seen in Fig. 6a, d. This type of growth mechanism quite reported in literature [47] is known as Oriented Attachment. This process consists in the growth of particles by crystallographic alignment and coalescence of neighboring particles by eliminating the common interface between particles while other particles have a disoriented growth. After nucleation, the particles tend to form aggregates due to Ostwald Ripening growth process (OR) [48]. The OR process occurs spontaneously so that the larger particles are energetically favored by the smaller particles resulting in the coalescence of the particles. These particles exhibit an anisotropic growth. According to Fig. 6e, the $PbMoO_4$ particles show a morphology similar to a micro - octahedron.

Increases attention to control of the morphology and size of particles obtained by chemical methods because these characteristics can affect its properties and performance compromise their technological applications. The crystal initially provides a primary level of agglomeration. The structure of $PbMoO_4$ consists of small crystals of a few nanometers. The growth rate of the crystals can is associated with saturation of the reaction medium, this behavior does not occur in a linear manner in previous studies.

Fig. 7 shows the average particle size distribution of $PbMoO_4$ particles processed in the sonochemistry method at different synthesis time.

It is observed a decrease in the average size of the particles due to the increase in time exposure by the ultrasound of 30–45 min $PbMoO_4$ particles treated by a sonochemical amplitude of 70% in 30 and 45 min showed a broad-range size distribution. Almost 34% of the particles synthesized at the 30 min time is between 0.75 and

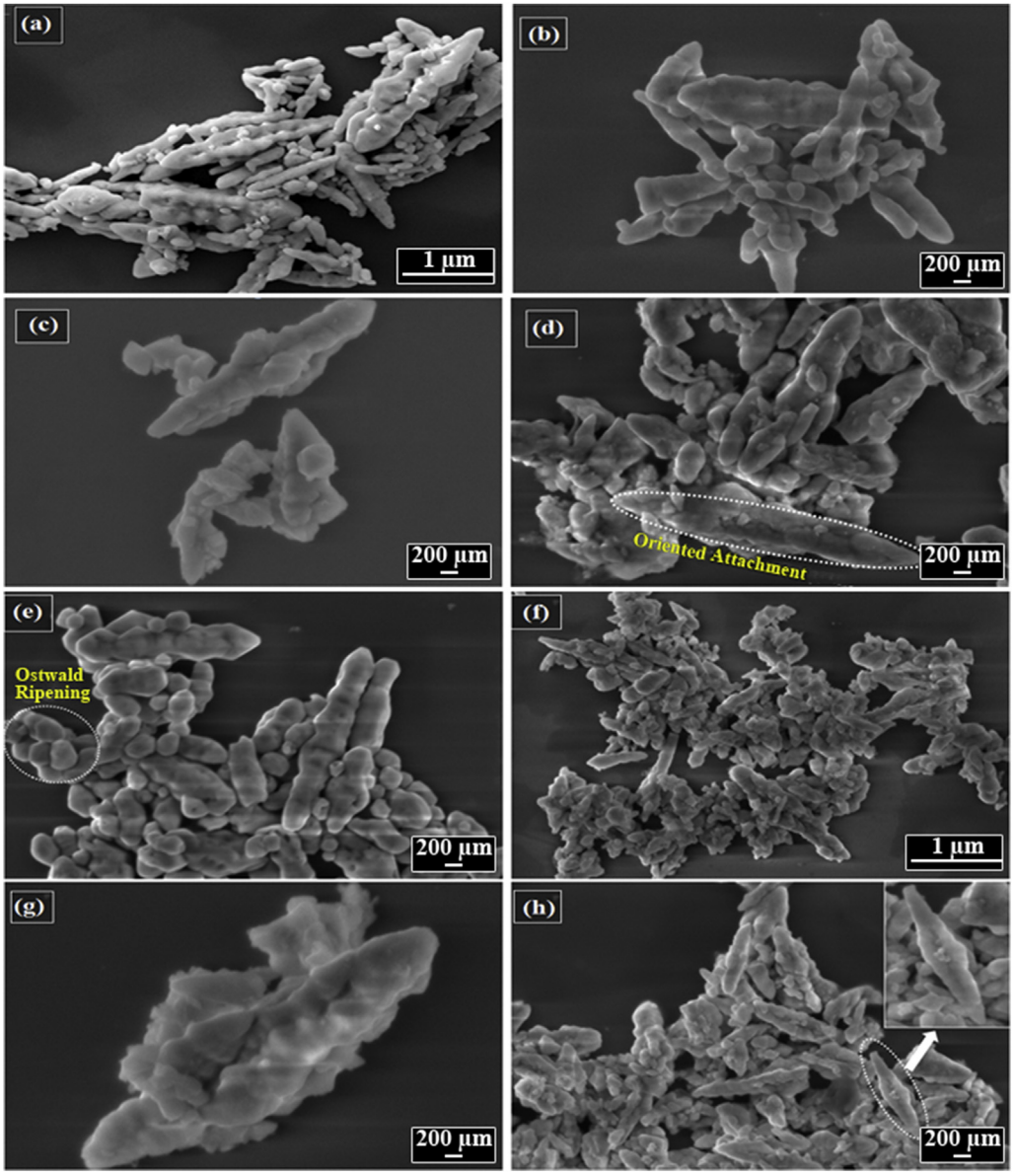

Fig. 6. SEM micrographs of $PbMoO_4$ pure and co-doped processed by sonoquímico method: (a) pure 30 min, (b) pure 45 min (c) 0.5% Eu 30 min (d) 0.5% Eu 45 min, (e) 1% Eu 30 min (f) 1% Eu 45 min, (g) 1.5% Eu 30 min and (h) 1.5% Eu 45 min.

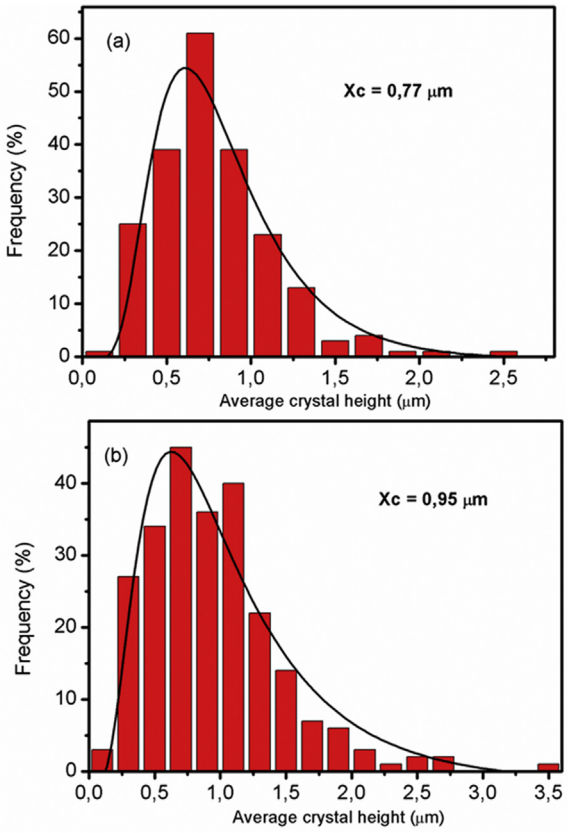

Fig. 7. Average particle size distribution of $PbMoO_4$ particles processed by the sonochemical method at (a) 30min and (b) 45min.

0.9 μm. For particles produced in 45min, 32% of them correspond to the size between 0.9 and 1.1 μm. This behavior has been discussed by Suslick and Price [49], who suggests that the propagation of shock waves may induce the sintering of solid particles of the solute in a liquid-solid system, from collisions between particles at straight angles.

Fig. 8 shows the schematic representation of the main growth mechanisms involved in the synthesis of $PbMoO_4$ crystals by the sonochemical method. The crystal growth is controlled by extrinsic and intrinsic factors, including the degree of supersaturation, diffusion of the reaction, surface energy, crystal structure, and solution parameters. Several well-known crystal growth mechanisms in the solution system are the oriented attachment, Ostwald ripening process.

The formation of small octahedral $PbMoO_4$ occurred from the dissolution of the precursors [H_2MoO_4 and $Pb(NO_3)_2$] in deionized water. This solution is a fast ionization and dissociation acid salt, the ions of Pb^{2+} and $(MoO_4)^{2-}$ are instantly solvated by H_2O molecules. The difference in the electron density between Pb^{2+} and $(MoO_4)^{2-}$ ions promotes the electrostatic attraction between them resulting in the precipitation/crystallization process (Fig. 8a). The increase in the precipitation rate is observed with the addition of NH_4OH solution to generating a disordered growth of the crystals due to a rapid process of self-assembly during the precipitation material. When the $PbMoO_4$ crystals are exposed to the irradiation of ultrasound, the energy supplied to the solution allows the dissolved crystals to start a recrystallization process (Fig. 8b), which is attributed to the cavitational effects resulting out of the high frequency irradiation. The crystals obtained in this stage have led to growth. Subsequently, $PbMoO_4$ particles have an anisotropic growth and formation of irregular micro-octahedrons. This growth mechanism is known as Ostwald Ripening, where small particles are less thermodynamically stable than larger ones. This coalescence occurs which promotes growth (Fig. 8c). The $PbMoO_4$ crystals show a growth model oriented in the crystallographic direction [001]. This type of crystal growth mechanism is called the Oriented Attachment. Fig. 8d shows the particles with dendritic structure. There is a main trunk and four cross arms extending from the center of the main trunk. Crossed branches build the structure of a perfect perpendicular. It is observed that the dendritic morphology constituted nanopolyedrons arranged which are connected to each other in an interesting way. This type of morphology is described in previous work [50,51].

4. Conclusions

In summary, this study explained that the particles of $PbMoO_4$ are obtained easily through sonoquímico method without the need for subsequent heat treatment. XRD results indicate that the crystals have tetragonal scheelite structure of the type without the presence of secondary phases. The variation of Egap between 3.18 and 3.24 eV is justified by the existence of intermediate levels in the band gap from the presence of the RE^{3+} $PbMoO_4$ lattice. This effect is favorable to facilitate the electronic transitions, optimizing the photoluminescent properties. The $PbMoO_4$ matrix presents a significant behavior in photoluminescence with discrete bands related to the transitions of type f → f of rare-earths. A broadband model was proposed to explain the emission PL allocated by charge transfer within the cluster [MoO_4] which there is as photoluminescence properties of $PbMoO_4$ are very sensitive to the structure and heavily dependent on structural defects. Agreements with chromaticity coordinates, the samples showed a predominant issue in green. The morphological evolution of the particles was examined, indicating an anisotropy of crystal growth through Ostwald Ripening and oriented Attachment mechanisms. The results of this work suggest that these materials have significant potential for use in the field of light-emitting diodes.

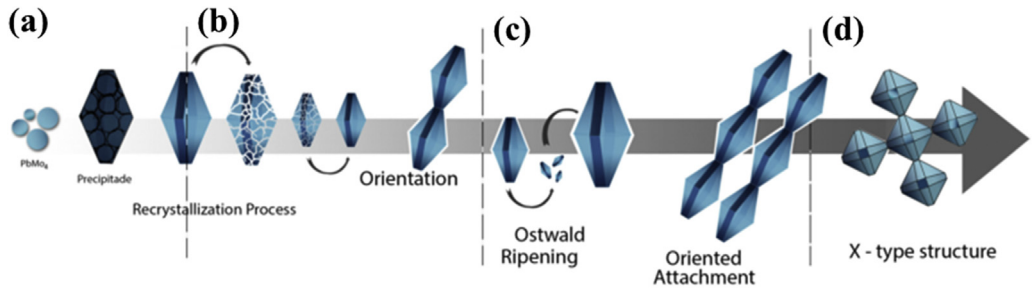

Fig. 8. A schematic illustration of the growth mechanism of $PbMoO_4$ crystals by the sonochemical method.

Acknowledgment

The authors gratefully acknowledge the financial support of the Brazilian governmental research funding agencies CAPES, CNPq 402127/2013-7, FAPESP 2013/07296-2 and INCTMN 2008/57872-1.

References

[1] V.D. Araújo, R.L. Tranquilin, F.V. Motta, C.A. Paskocimas, M.I.B. Bernardi, L.S. Cavalcante, J. Andres, E. Longo, M.R.D. Bomio, Effect of polyvinyl alcohol on the shape, photoluminescence and photocatalytic properties of $PbMoO_4$ microcrystals, Mat. Sci. Semicond. Proc. 26 (2014) 425–430.
[2] J. Liu, P.J. Lu, S.Q. Liang, J. Liu, W.J. Wang, M. Lei, Ultrathin Li3VO4 nanoribbon/graphene sandwich-like nanostructures with ultrahigh lithium ion storage properties, Nano Energy 12 (2015) 709–724.
[3] D.B. Hernández-Urestia, A. Martínez-de la Cruzb, L.M. Torres-Martínezc, Photocatalytic degradation of organic compounds by $PbMoO_4$ synthesized by a microwave-assisted solvothermal method, Ceram. Int. 42 (2016) 3096–3103.
[4] S. Huang, J.G. Li, X. Wang, Q. Zhu, X. Sun, Controlled synthesis and the effects of Gd^{3+} substitution, calcination and particle size on photoluminescence of $(Y_{0.95x}Gd_xTb_{0.05})_2O_3$ green phosphor spheres, Chem. Eng. Commun. 306 (2016) 322–329.
[5] J. Zhang, T. Zhao, L. Zou, Ultrasound-assisted precipitation synthesis of $PbMoO_4$ and $PbMoO_4$:Eu^{3+} nanocrystals and photoluminescence properties, J. Photochem. Photobiol. A 314 (2016) 35–41.
[6] Y. Zhiyong, D. Chaonan, Q. Ruiying, X. Lijin, Photocatalytic degradation of methyl orange by $PbXO_4$(X = Mo, W), J. Colloid Interface Sci. 438 (2015) 323–331.
[7] L. Wang, H. Tang, Y. Tian, Carbon-shell-decorated *p*-semiconductor $PbMoO_4$ nanocrystals for efficient and stable photocathode of photoelectrochemical water reduction, J. Power Sources 319 (2016) 210–218.
[8] C. Guo, J. Xu, S. Wang, L. Li, Y. Zhang, X. Li, Facile synthesis and photocatalytic application of hierarchical mesoporous Bi_2MoO_6 nanosheet-based microspheres, Cryst. Eng. Comm. 14 (2012) 3602–3608.
[9] F.Z. Duan, C. Yan, Q. Ming, Enhanced photocatalytic activity of bismuth molybdate via hybridization with carbon, Mater. Lett. 65 (2011) 191–193.
[10] D.B. Hernández-Uresti, A. Martínez-de la Cruz, J.A. Aguilar-Garib, Photocatalytic activity of $PbMoO_4$ molybdate synthesized by microwave method, Catal. Today 212 (2013) 70–74.
[11] M.R.D. Bomio, L.S. Cavalcante, M.A.P. Almeida, R.L. Tranquilin, N.C. Batista, P.S. Pizani, M. Siu Li, J. Andres, E. Longo, Structural refinement, growth mechanism, infrared/Raman spectroscopies and photoluminescence properties of $PbMoO_4$ crystals, Polyhedron 50 (2013) 532–545.
[12] M.C. Oliveira, L. Gracia, I.C. Nogueira, M.F. do C. Gurgel, J.M.R. Mercury, E. Longo, J. Andrés, Synthesis and morphological transformation of $BaWO_4$ crystals: experimental and theoretical insights, Ceram. Int. 42 (2016) 10913–10921.
[13] M. Bazarganipour, Synthesis and characterization of $BaMoO_4$ nanostructures prepared via a simple sonochemical method and their degradation ability of methylene, Ceram. Int. 42 (2016) 12617–12622.
[14] L.L. He, X.P. Liu, Y.X. Wang, Z.X. Wang, Y.J. Yang, Y.P. Gao, B. Liu, X. Wang, Sonochemical degradation of methyl orange in the presence of Bi_2WO_6: effect of operating parameters and the generated reactive oxygen species, Ultrason. Sonochem. 33 (2016) 90–98.
[15] L. Yang, Y. Wang, X. Wang, G. Han, Shape-controlled of $CaWO_4$ microcrystals by self-assembly of nanocrystals via a simple sonochemical method, Adv. Powder Technol. 24 (2013) 721–726.
[16] L. Zhu, J. Meng, X.Q. Cao, Sonochemical synthesis of monodispersed KY_3F_{10}:Eu^{3+} nanospheres with bimodal size distribution, Mater. Lett. 62 (2008) 3007–3009.
[17] R.K. Selvan, A. Gedanken, P. Anilkumar, G. Manikandan, C. Karunakaran, Synthesis and characterization of rare earth orthovanadate (RVO_4; R = La, Ce, Nd, Sm, Eu and Gd) nanorods/nanocrystals/nanospindles by a facile sonochemical method and their catalytic properties, J. Clust. Sci. 20 (2009) 291–305.
[18] C.S. Lim, Highly modulated structure and upconversion photoluminescence properties of $PbGd_2(MoO_4)_4$:Er^{3+}/Yb^{3+} phosphors, Mater. Res. Bull. 75 (2016) 211–216.
[19] S. Vidya, J.K. Thomas, Study on the optical band gap and photoluminescence of $PbMoO_4$ nano powder synthesized by an auto igniting combustion technique, Mater. Sci. Eng. 73 (2015) 012120–012122.
[20] Z. Yan, Y. Tang, B. Sun, T. Liu, X. Li, P.S. Ping, X. Yu, Y. Zhang, Q.J. Wang, Switchable multi-wavelength Tm-doped mode-locked fiber laser, Opt. Lett. 40 (2015) 1916–1919.
[21] X. Zhang, Z. Zhao, J. Chaudhuri, In-situ crystal growth and photoluminescence properties of YBO_3: Tb^{3+}microstructures, J. Mater. Sci. 50 (2015) 251–257.
[22] Y.S. Vidya, K.S. Anantharaju, H. Nagabhushana, S.C. Sharma, H.P. Nagaswarup, S.C. Prashantha, C. Shivakumara, Combustion synthesized tetragonal ZrO2:Eu^{3+} nanophosphors: structural and photoluminescence studies, Spectrochim. Acta Mol. Biomol. Spectrosc. 135 (2015) 241–251.
[23] J. Zhang, L. Li, W. Zi, N. Guo, L. Zou, S. Gan, G. Ji, Self-assembled $CaMoO_4$ and $CaMoO_4$:Eu^{3+} hierarchical superstructures: facile sonochemical route synthesis and tunable luminescent properties, J. Phys. Chem. Solids 75 (2014) 878–887.
[24] E.F. Schubert, Light Emitting Diodes, Cambridge University Press, 2003.
[25] R. Robertson, Computation of correlated color temperature and distribution temperature, J. Opt. Soc. Am. 58 (1968) 1528–1535.
[26] L.F. Santos, C.J. Pereira, Dithering by radiometric and photometric calibration LEDs: theory and experiment, Rev. Bras. Ensino Física 35 (2013) 2314.
[27] D. Tawde, M. Srinivas, K.V.R. Murthy, Effect of lead source and cerium (III) doping on structural and photoluminescence properties of $PbWO_4$ microcrystallites synthesized by hydrothermal method, Phys. Status Solidi A 208 (2011) 803–807.
[28] P. Kubelka, F. Munk, Ein beitrag zur optik der farbanstriche, Z. Phys. 12 (1931) 593–601.
[29] R.L. Perales, J.R. Fuertes, D. Errandonea, A. Segura, Optical absorption of divalent metal tungstates: correlation between the band-gap energy and the cation ionic radius, Eur. Phys. Lett. 83 (2008) 37002–37006.
[30] R. Gonçalves, L. Cavalcante, I. Nogueira, E. Longo, M. Godinho, J. Sczancoski, V. Mastelaro, I. Pinatti, I. Rosa, A. Marques, Rietveld refinement, cluster modelling, growth mechanism and photoluminescence properties of CaWO4: Eu3+ microcrystals, Cryst. Eng. Comm. 17 (2015) 1654–1666.
[31] D.C. Cronemeyer, Infrared absorption of reduced rutile TiO_2 single crystals, Phys. Rev. 113 (1959) 1222–1226.
[32] J.C. Sczancoski, M.D.R. Bomio, L.S. Cavalcante, M.R. Joya, P.S. Pizani, J.A. Varela, E. Longo, M.S. Li, J.A. Andrés, Morphology and blue photoluminescence emission of $PbMoO_4$ processed in conventional hydrothermal, J. Phys. Chem. C 113 (2009) 5812–5822.
[33] F. Lei, B. Yan, H. Chen, Q. Zhang, J. Zhao, Surfactant-assisted hydrothermal synthesis, physical characterization and photoluminescence of $PbWO_4$, Cryst. Growth Des. 9 (2009) 3730–3736.
[34] J. Geng, J. Zhu, D. Lu, H. Chen, Hollow $PbWO_4$ nanospindles via a facile sonochemical route, Inorg. Chem. 45 (2006) 8403–8407.
[35] G. Blasse, B.C. Grabmaier, Luminescent Materials, Springer, Berlin, 1994.
[36] A.B. Campos, et al., Mechanisms behind blue, green and red photoluminescence emissions in $CaWO_4$ and $CaMoO_4$ powders, Appl. Phys. Lett. 91 (2007) 051923–051925.
[37] D.A. Spassky, et al., Optical and luminescent properties of the lead and barium molybdates, Radiat. Meas. 38 (2004) 607–610.
[38] Z. Wang, Y. Li, X. Liu, X. Wei, Y. Chen, F. Zhou, Y. Wang, Photoluminescence performance of thulium doped $Li_4SrCa(SiO_4)_2$ under irradiation of ultraviolet and vacuum ultraviolet lights, Mater. Res. Bull. 59 (2014) 295–299.
[39] J. Li, C. Deng, R. Cui, Photoluminescence properties of $CaBi_2Ta_2O_9$:RE^{3+} (RE = Sm, Tb and Tm) phosphors, Opt. Commun. 326 (2014) 6–9.
[40] M. Mohapatra, B. Rajeswari, N.S. Hon, R.M. Kadam, V. Natarajan, Photoluminescence properties of 'red' emitting $La_2Zr_2O_7$:Eu pyrochlore ceramics for potential phosphor application, J. Lumin 166 (2015) 1–7.
[41] X. Wu, et al., Aqueous mineralization process to synthesize uniform shuttle-like $BaMoO_4$ microcrystals at room temperature, J. Solid State Chem. 180 (2007) 3288–3295.
[42] W. Vanloo, Luminescence of lead molybdate and lead tungstate, I. Exp. Phys. Status Solidi A 27 (1975) 565–574.
[43] W. Vanloo, Luminescence decay of lead molybdate and tungstate - a descriptive model, J. Lumin 10 (1974) 221–235.
[44] W. Vanloo, Luminescence of lead molybdate and lead tungstate, Ii. Discuss. Phys. Status Solidi A 28 (1975) 227–235.
[45] J.H. Ryu, et al., Microwave-assisted synthesis of $BaMoO_4$ nanocrystallites by a citrate complex method and their anisotropic aggregation, J. Alloys Compd. 413 (2006) 144–149.
[46] J. Yang, C. Lu, H. Su, J. Ma, H. Cheng, L. Qi, Morphological and structural modulation of $PbWO_4$ crystals directed by dextrans, Nanotechnology 19 (2008) 035608–035615.
[47] S. Jia, H. Zheng, H. Sang, W. Zhang, H. Zhang, L. Liao, J. Wang, Self-assembly of K_xWO_3 nanowires into nanosheets by an oriented attachment mechanism, ACS Appl. Mater. Interfaces 5 (2013) 10346–10351.
[48] M. Shen, Q. Zhang, H. Chen, Hydrothermal fabrication of PbMoO4 microcrystals with exposed (001) facets and its enhanced photocatalytic properties, Cryst. Eng. Comm. 13 (2011) 2785–2791.
[49] K.S. Suslick, G.J. Price, Applications of ultrasound to materials chemistry, Annu. Rev. Mater. Sci. 29 (1999) 295–326.
[50] Y. Tian, et al., Ionic liquid-assisted hydrothermal synthesis of dendrite-like $NaY(MoO_4)_2$:Tb^{3+} phosphor, Phys. B 407 (2012) 2556–2559.
[51] Y. Cheng, Y. Wang, D. Chen, F. Bao, Evolution of single crystalline dendrites from nanoparticles through oriented attachment, J. Phys. Chem. B 109 (2005) 794–798.